Diabetes in a Dish: Modeling and Phenotyping Acute and Chronic Type 2 Diabetes Mellitus In Vitro in Rodent Heart and Skeletal Muscle Cells

Elena Luise Kopp , Daniel Nils Deussen , Raphael Cuomo , Reinhard Lorenz , David M Roth , Sushil K. Mahata , Hemal H Patel *

Posted Date: 8 November 2023

doi: 10.20944/preprints202310.0319.v2

Keywords: Insulin resistance; type 2 diabetes; cell model; mitochondrial dysfunction

Article

Modeling and Phenotyping Acute and Chronic Type 2 Diabetes Mellitus In Vitro in Rodent Heart and Skeletal Muscle Cells

Elena L. Kopp [1,2], Daniel N. Deussen [1,2], Raphael Cuomo [1], Reinhard Lorenz [3], David M. Roth [1,5], Sushil K. Mahata [4,5] and Hemal H. Patel [1,5,*]

[1] Department of Anesthesiology, University of California San Diego, La Jolla, California, United States of America
[2] University of Munich (LMU Munich), Munich, Germany
[3] Institute for Cardiovascular Prevention (IPEK), LMU Munich, Munich, Germany
[4] Department of Medicine, University of California, San Diego, CA 92093
[5] VA San Diego Healthcare System, San Diego, CA 92161
* Correspondence: Hemal H. Patel, PhD, VA San Diego Healthcare System and Department of Anesthesiology, University of California, San Diego, #125, 3350 La Jolla Village Dr., San Diego, CA 92161, Email: hepatel@ucsd.edu

Abstract: Type 2 diabetes (T2D) has a complex pathophysiology which makes modeling the disease difficult. We aimed to develop a novel model for simulating T2D in vitro, including hyperglycemia, hyperlipidemia, and variably elevated insulin levels targeting muscle cells. We investigated insulin resistance (IR), cellular respiration, mitochondrial morphometry and the associated function in different T2D -mimicking conditions in rodent skeletal (C2C12) and cardiac (H9C2) myotubes. Physiological controls included 5mM glucose with 20mM mannitol as osmotic controls. To mimic hyperglycemia, cells were exposed to 25mM glucose. Further treatments included insulin, palmitate, or both. After short-term (24h) or long-term (96h) exposure, we performed radioactive glucose uptake and mitochondrial function assays. Mitochondrial size and relative frequencies were assessed by morphometric analyses using electron micrographs. C2C12 and H9C2 cells treated short- or long-term with insulin and/or palmitate and HG showed IR. C2C12 myotubes exposed to T2D -mimicking conditions showed significantly decreased ATP-linked respiration and spare respiratory capacity, and less cytoplasmic area occupied by mitochondria, implying mitochondrial dysfunction. In contrast, H9C2 myotubes showed elevated ATP-linked and maximal respiration and increased cytoplasmic area occupied by mitochondria, indicating better adaptation to stress and compensatory lipid oxidation in a T2D environment. Both cell lines displayed elevated fractions of swollen/vacuolated mitochondria after T2D -mimicking treatments. Our stable and reproducible in vitro model of T2D rapidly induced IR, changes in ATP-linked respiration, shifts in energetic phenotypes, and mitochondrial morphology, which are comparable to the muscles of patients suffering from T2D. Thus, our model should allow studying disease mechanisms, potential new targets, and screen candidate therapeutic compounds.

Keywords: insulin resistance; type 2 diabetes; cell model; mitochondrial dysfunction

1. Introduction

Diabetes mellitus (DM) represents a large global disease burden with an ominous prognosis [1]. It is predicted that more than 550 million people worldwide will be diabetic by 2030, compared to 108 million in 1980 [2]. Diabetes is among diseases with the most rapidly increasing global prevalence and improving therapies and prevention methods to reduce diabetes-related complications and premature mortality is of utmost importance.

 doi:10.20944/preprints202310.0319.v2

DM is characterized by a relative or absolute lack of insulin, resulting in elevated blood glucose levels. Type 2 diabetes (T2D) accounts for more than 90% of DM cases and is primarily caused by an inappropriate cellular response to insulin. In response to insulin resistance (IR) or intolerance, pancreatic beta cells hypertrophy and release more insulin, consequently leading to pancreatic exhaustion and failure in later stages of the disease [3]. The natural history of T2D is characterized by obesity in >80% of cases, which is further exacerbated by a Western diet and physical inactivity leading to IR, hyperglycemia, hyperlipidemia, and hyperinsulinemia [4]. Chronic hyperglycemia can lead to microvascular (e.g., nephropathy, retinopathy, and polyneuropathy) and macrovascular (e.g., stroke, cardiovascular disease) complications [5]. In T2D patients, cardiovascular disease is a major cause of morbidity and mortality, accounting for 68% of all diabetes-related deaths [6].

Given the physiological complexity of the disease, in vitro models that could provide a path to discovery and testing of novel therapeutics have been limited. By modeling this complex disease *in vitro,* we want to increase and accelerate the discovery of therapeutic targets, improve disease screening, and enable improved preclinical drug testing. In vitro cell models can provide an economically and ethically acceptable research tool and enable the targeting of specific processes linked to a single cell type of interest, without uncontrolled influences of the whole organism. In vitro cell models can be performed with high throughput and reproducibility and can be genetically modified by transfection to investigate specific genes of interest [7]. Thus, cell-based models, if developed properly, could serve as tools to accelerate therapeutic discovery.

In general, in vitro models of diabetes are derived from the tissues that are mainly involved in the disease pathophysiology, such as muscle, pancreas, adipose tissue, and liver [8]. Skeletal muscle is the primary recipient of postprandial glucose, and T2D patients often show significantly impaired blood glucose clearance [9]. Also, the higher flux of FFAs in patients with T2D leads to an increased FA-uptake into myocytes [10]. To assess the effect of T2D on skeletal muscle, we chose to use C2C12 cells, a mouse myoblast cell line, which is well-established and has been widely used in diabetes research [11]. In the setting of IR, the myocardium's ability to utilize glucose as an energy source is reduced [12], whereas under physiological conditions energy utilization from FA and carbohydrates is based on metabolic demand and availability [13]. Even though FFAs are the major energy source for heart muscle, an excess of plasma FFAs may predispose the heart to ischemic damage and high oxidative stress [14]. These metabolic changes and the accumulation of lipids in the heart play a critical role in the development of diabetes-related cardiac complications, such as diabetic cardiomyopathy [15,16]. To further understand these mechanisms in heart muscle, we mimicked diabetic conditions in H9C2 cells, which are myocytes from embryonic rat ventricular tissue [17]. H9C2 myocytes are widely applied in studies addressing cardiac hypertrophy, metabolism, ischemic stress, and IR/diabetes [18,19].

To cause IR as it is occurring in T2D, most cell models with adipocytes and myocytes use chronic insulin exposure or fatty acid treatments (mainly palmitate) [20] (Table 1). The most commonly used immortalized muscle cell lines for in vitro diabetes models are L6 and C2C12 myoblasts [21].

Table 1. Selection of current in vitro models of type 2 diabetes and insulin resistance.

Cell type and differentiation	Preincubation	Type of treatment, concentration, duration	Read outs	Reference
3T3-L1 adipocytes	DMEM 5 mM glucose	Palmitate 0.75 mM 17h Hypoxia 16h Dexamethasone 1 µmol/l 24h	Inhibition of phosphorylation of insulin receptor and protein kinase B; decrease in insulin dependent glucose uptake	[20] [22] [23]

Preprints (www.preprints.org) | NOT PEER-REVIEWED | Posted: 8 November 2023 doi:10.20944/preprints202310.0319.v2

		High glucose 25 mM 18h	Impaired GLUT4 membrane intercalation	[24]
C2C12 myoblasts	DMEM 25 mM glucose	Insulin 60 nM 24h Palmitate 0.4 mM 24h	Inhibition of insulin stimulated activation of Akt/protein kinase B; Swollen mitochondria	[21]
	DMEM 5 mM glucose	Glucose 15 mM 24h Palmitate 0.25 mM 24h	Increased apoptosis, increased ROS production	[25]
C2C12 myotubes	DMEM 5 mM glucose	Palmitate 0.75 mM 17h	Inhibition of insulin stimulated glycogen synthesis and activation of protein kinase B, diacylglyceride accumulation	[20]
	DMEM not specified	Palmitate 0.6 mM 24h	Reduced Akt phosphorylation, glucose uptake and GLUT4 expression	[26]
Huh7 differentiated hepatocellular carcinoma	DMEM 25 mM glucose	Insulin 60 nM 24h Palmitate 0.4 mM 24h	Inhibition of insulin stimulated activation of Akt/protein kinase B	[21]
Primary human myotubes	DMEM not specified	Palmitate 0.5 mM 48h	Decrease in insulin stimulated glucose uptake	[27]
H9C2 myoblasts	DMEM 25 mM glucose	Glucose 33 mM 36h	Enhanced apoptosis, activation of cardiac hypertrophy proteins	[28]
		Glucose 40 mM 24h	Increased ROS production + apoptosis	[29] [30]
	DMEM 5 mM glucose	Glucose 25 mM + insulin 100 nM 24h	Decrease in insulin stimulated glucose uptake, Inhibition of insulin stimulated activation of Akt	
H9C2 myotubes	DMEM not specified	Palmitate 100 µM 24h	Decrease in insulin stimulated glucose uptake	[31]

To simulate the diabetic milieu *in vitro*, not only the cells themselves play a critical role, but also the conditions in which they are cultured. The main reason for metabolic syndrome and T2D is chronic overnutrition consisting mainly of fatty acids and carbohydrates in the developed world [32].

 doi:10.20944/preprints202310.0319.v2

In vitro studies showed that once a cell becomes overwhelmed by the excess supply of FFAs, the accumulation of lipids such as diacylglyceride (DAG) and ceramide may contribute to mitochondrial dysfunction, generation of reactive oxygen species (ROS), low-grade inflammation, and finally IR and apoptosis [33]. Correspondingly, symptoms of T2D are caused by both hyperglycemia and hyperlipidemia, whereas hyperglycemia alone would more likely reflect uncontrolled T1D [34]. In cell culture research, it is a common practice to use culture media with supraphysiological glucose concentrations to promote and accelerate cellular growth. Previous studies addressing IR and diabetes in H9C2 and C2C12 muscle cells worked with 22-25 mM glucose as control and 33-40 mM glucose to mimic hyperglycemia, which is 8 times more than physiological levels [28,29]. In several studies investigating DM, glucose concentrations of cell culture media are not specified, leaving the reader uninformed (Table 1) [26,27,31]. The American Diabetes Association and WHO define normoglycemia as a fasting plasma glucose between 3.9 mmol/L and 5.6 mmol/L [35,36]. Diabetes is defined when the fasting plasma glucose reaches 7.0 mmol/L or higher [37]. It is recommend to first growing and differentiating cells in physiological glucose levels of 5 mM [25]. The simulation of hyperlipidemia requires the treatment with fatty acids (FA). Chavez and Summers showed that the saturated FA palmitate (the most dominant fat in the western fast food diet) causes IR, whereas unsaturated FAs such as oleate even reversed palmitate-induced IR in skeletal muscle [20]. This suggests using the widely applied FA palmitate for T2D-related hyperlipidemia conditions. High concentrations of palmitate (200-750 μM), which have previously been used in studies investigating IR, can cause apoptosis and high myotube loss in skeletal and cardiac muscle cells [26,38,39]. We therefore worked with a maximal concentration of 150 μM for C2C12 and 75 μM for H9C2, which still leads to IR but is less toxic and close to the physiological range (300-410 μM in humans [40] and 100-400 μM in rats [41]). In conclusion, exposure to high glucose, palmitate, and insulin together, may be closer to conditions observed in T2D patients compared to previously described cell-based approaches (Table 1). To achieve more similarity to human muscle tissue we worked with differentiated myotubes, whilst many research groups work with the undifferentiated myoblasts [25,42,43]. The insulin dependent glucose transporter 4 (GLUT4) is similarly expressed in C2C12 myotubes compared to human skeletal muscle cells [11]. Undifferentiated H9C2 myoblasts express little cardiac specific markers and can still differentiate into skeletal muscle instead of cardiac muscle. In 2017 Patten et al. stated that the combination of serum reduction with retinoic acid (RA) supplementation in the differentiation process did increase the expression of cardiac specific markers [44]. Lopashuk et al. identified that only differentiated H9C2 cells switch from glycolysis to oxidative phosphorylation, which is characteristic for heart tissue [45]. Also, insulin-signaling molecules such as insulin receptor substrate-1 and GLUT4 are significantly more expressed by differentiated H9C2 myotubes [46]. In conclusion, differentiation into myotubes to explore heart and skeletal muscle specific processes related to T2D is necessary. Various human studies suggested the existence of mitochondrial dysfunction in muscle cells of obese and insulin-resistant patients [47,48]. Comprehensive understanding of the mechanisms that relate mitochondrial function and insulin signaling is still lacking. Identifying the factors and mechanisms responsible for changes in mitochondrial energetics could make mitochondria to a potential target for treating diabetes. Therefore, we examined mitochondrial function in vitro in rodent skeletal and heart muscle utilizing the Agilent Seahorse XF Analyzer and utilized transmission electron microscopy (TEM) to examine mitochondrial morphometry.

Taken together, this study aimed to develop a novel model for simulating T2D in vitro in skeletal and cardiac muscle cells that reflects the cellular response typified by T2D patients.

2. Materials and Methods

2.1. Cell culture

C2C12 (CRL-1772™) and H9C2 (CRL-1446™) cell lines were purchased from American Type Culture Collection (ATCC, Manassas, VA, USA). C2C12 and H9C2 cells were cultured in Dulbecco's Modified Eagle's Medium (DMEM) (GIBCO/BRL, 11885092) containing 5 mM glucose, supplemented

 doi:10.20944/preprints202310.0319.v2

with 10% fetal bovine serum (FBS, Thermo Fisher Scientific, 16000044) and 1% penstrep (Penicillin/Streptomycin, GIBCO, 15140122). For differentiation of C2C12, DMEM (5 mM glucose) was supplemented with 2% horse serum (HS) (Thermo Fisher, 26050088) and 1% penstrep was refreshed daily. For differentiation of H9C2 cells, DMEM (5 mM glucose) was supplemented with 1% FBS, 1% penstrep and 10nM All-trans-retinoic acid (RA) (Sigma Aldrich, R2625-500MG). RA was diluted in DMSO and stored at -20°C in the dark. Medium change was performed daily in the dark. Cell treatments for assays were started 5-8 days after differentiation. C2C12 and H9C2 cell cultures were used in passages 2-6 in all experiments.

2.2. Treatments

DMEM containing 25 mM glucose (GIBCO/BRL, 11995073) was used as a hyperglycemic condition (HG). This hyperglycemic condition was also used in combination with insulin (HG-I) (1 nM, insulin glargine, Lantus, Sanofi), or palmitate (HG-P) (150 µM for C2C12, 75 µM for H9C2). A further hyperglycemic condition was combined with both insulin and palmitate (HG-PI). Groups treated with low glucose (LG, 5 mM) and the same combinations with palmitate and/or 1 nM insulin served as physiological controls (LG-I, LG-P, LG-PI). To exclude a possible hyperosmolar effect, cells treated with 20 mM mannitol plus 5 mM glucose served as control cultures (high mannitol, HM). The same treatment combinations were used (HM-I, HM-P, HM-PI). The cells were exposed to different conditions, either short-term (24h) or long-term (96h). Before all experiments, the culture medium was changed to serum-free medium for 4 hours. For long-term treatments, the concentration of palmitate was escalated every 24 hours to prevent myotube loss (Table 2).

Table 2. Escalation of palmitate concentrations for long term (96h) treatments of C2C12 and H9C2 myotubes. Palmitate concentrations were increased every 24 hours.

Treatment duration	Conc. For C2C12	Conc. For H9C2
24h	35 µM	5 µM
48h	70 µM	25 µM
72h	105 µM	50 µM
96h	150 µM	75 µM

Before adding sodium palmitate to cell differentiation medium, it was conjugated to fatty acid free bovine serum albumin (BSA). Transportation into cells is then enabled and cytotoxicity lowered. Briefly, ultra-fatty acid free BSA (Sigma Aldrich, A8806) was dissolved in the respective differentiation medium for each cell line, heating the solution to approximately 37°C. Sodium palmitate (Sigma Aldrich, P9767) was dissolved in a 150 mM NaCl solution, stirring at 70°C. The palmitate solution was added to the BSA solution while stirring at 37°C. After stirring for 1 h, pH was adjusted to 7.4 with NaOH. The conjugated palmitate-BSA solution was aliquoted in glass vials and frozen at -20°C. Stock solutions were made at 75 mM.

2.3. ^{3}H-2-deoxy-glucose-uptake

^{3}H-2-deoxy-glucose-uptake assays were performed using published methods [49]. Briefly, culture media were discarded 4 hours prior to the assay and changed to serum-free DMEM with 0.25% fatty acid-free BSA. Serum-Starvation was held in respective treatment media (serum-free DMEM with either high or low glucose (5 mM vs 25 mM) and supplemented with palmitate or 1 nM insulin respectively). After starvation cultures were washed twice with Hepes fortified Krebs-Ringer Bicarbonate buffer (HKRB), containing 10 mM Hepes, pH 7.4, NaH2PO4 (0.83 mM), Na2HPO4 (1.27 mM), NaHCO3 (15 mM), NaCl (120 mM), KCl (4.8 mM), calcium (1 mM), magnesium (1mM), pH 7.35 and 0.25% fatty acid-free BSA. Cultures were incubated in HKRB for 60 minutes at 37°C. Half of the cultures were pre-assigned for acute insulin treatment. These cultures were treated with 100 nM insulin from a 100x stock and incubated for 20 minutes at 37°C. After this incubation period ^{3}H-2-deoxy-glucose (^{3}H-2DOG, 2-[1,2-3H(N)]-, 250µCi (9.25MBq), Perkin Elmer, NET549A250UC) was

 doi:10.20944/preprints202310.0319.v2

added to each well for further 10 minutes incubation. ^{3}H-2DOG-treatment was terminated by quick aspiration, followed by cold wash (2x) with ice-cold PBS. Next, we added 1N NaOH and swirled the plates slowly for 30 minutes to dissolve the cells. Aliquots of 20 µl were taken out of each well for protein measurements. The whole lysate of each well was transferred into a scintillation vial. After neutralizing NaOH with 1N HCl, scintillation cocktail (Ecoscint original, National Diagnostics, LS-271) was added and radioactivity was measured. Results were normalized with protein concentrations and presented as counts per minute (cpm) per mg protein. Alternately, the results were presented as cpm per million cells.

2.4. Mitochondrial function measurements

Mitochondrial function measurements were performed with the Agilent Seahorse XFe 96 Extracellular Flux Analyzer (Agilent Technologies, La Jolla, California). The analyzer measures real time extracellular acidification rate (ECAR) and oxygen consumption rate (OCR) of cells. C2C12 and H9C2 cells were seeded and differentiated in a density of ~1.2 x10^{4} cells per well, and the Seahorse XF Mito Stress Test assay was carried out as previously described [50]. During the assay, inhibitors of mitochondrial function are injected sequentially to distinguish the following parameters: Basal respiration: Oxygen consumption used to meet cellular ATP demand under baseline conditions. It can be set by the rate of ATP utilization and substrate availability and oxidation. ATP-linked respiration: Upon injection of the ATP synthase inhibitor oligomycin a decrease in OCR represents the part of basal respiration that accounts for ATP-linked respiration, meeting the energetic needs of the cell. It is largely set by the ATP demand of the cell and substrate oxidation, which can be decreased if there is mitochondrial dysfunction. Maximal respiration: By adding the uncoupler carbonyl cyanide p-(trifluoromethoxy) phenylhydrazone (FCCP) the maximal OCR can be attained. FCCP mimics an "energy demand" and stimulates the respiratory chain to operate at maximum capacity and substrates are rapidly oxidized. It is also set by substrate supply and oxidation including the functional substrate transport across the plasma and mitochondrial membranes. Changes may reflect membrane defects, altered mitochondrial biogenesis and function and decreased oxidation abilities. Spare respiratory capacity: This value can be calculated with basal and maximal respiration values. It indicates the cell's capability to respond to an energetic demand and can be an indicator of cell fitness or flexibility. A decreased capacity can be linked to mitochondrial dysfunction but can also reflect an increased ATP demand/increased basal respiration (i.e., highly proliferative cells). Increases may reflect high substrate provision or enhanced oxidative capacity [51]. We plotted OCR versus ECAR values on an energy map to provide a qualitative measurement of the relative utilization of oxidative (OCR) versus glycolytic (ECAR) pathways for energy production.

2.5. Electron microscopy

C2C12 and H9C2 myotubes maintained short-term (24h) and long-term (96h) in different T2D-mimicking and control conditions (see: treatments) were fixed and embedded for electron microscopy (EM) as previously described [52]. Grids were viewed using a Jeol JEM1400-plus Transmission Electron Microscope and photographed with a Gatan OneView digital camera with 4k x 4k resolution.

2.6. Morphometric analyses of mitochondria

Using the free-hand tool of NIH ImageJ, we manually traced around the mitochondria to determine mitochondrial area and length as described previously [53]. Cytoplasmic area (excluding the area occupied by the nucleus) was also calculated using the ImageJ software. We then calculated mitochondrial density (area occupied by mitochondria in total area of cytoplasm). Mitochondrial numbers were calculated by placing the EM micrographs onto a grid with 10 horizontal x 10 vertical square grids followed by dividing the mitochondrial numbers with the area. The data were expressed as mitochondrial number/10 µm2 area.

 doi:10.20944/preprints202310.0319.v2

2.7. Statistical analysis

All Data analyses were performed using GraphPad Prism 9.5.1 (GraphPad Software, La Jolla, CA). For glucose uptake assays the results are expressed as mean ± SD of 6 biological replicates for all LG and HG groups and 3 replicates for all HM groups. For Mito Stress Tests, all data shown are the means ± SD of 3-4 replicate plates with 8-15 wells per treatment group per plate. Relative frequencies of mitochondria area and length were analyzed by Kolmogorov-Smirnov test, mitochondrial number, and density were analyzed by one-way ANOVA, of 6-14 cells. For statistical analysis a p value <0.05 was considered significant. We used analysis of variance (one-way or two-way ANOVA), provided that the assumptions were fulfilled. For Agilent Seahorse measurements two-way ANOVA was used with row factor for treatment groups (Rf) and column factor for biological replicates/assays (Cf). F- and p values are provided in the legend of the figure panels. Significance of secondary pairwise comparisons among different treatments by Tukey's test is indicated by asterisks over brackets in the figure panels (*: $p<0.05$; **: $p<0.01$; ***: $p<0.001$).

3. Results

3.1. ^{3}H-2-deoxy-glucose-uptake

C2C12 myotubes: We found that treatment of C2C12 myotubes with T2D-mimicking conditions including insulin and palmitate treatments resulted in IR compared to controls. Control cultures preincubated with LG for 24h showed a significant increase in glucose uptake upon stimulation with 100 nM test insulin (Figure 1A) (LG +/- insulin). Short-term (24h) pretreatments with 150 µM palmitate either in presence or absence of 1 nM insulin impeded the stimulatory effect of insulin, indicating that palmitate caused IR in consistence with existing literature [54]. Similar effects were seen after 96h (Figure 1K). After short- and long-term treatment, basal glucose uptake was increased in LG-I treated groups compared to LG controls (Figure 1A,K). LG-P and LG-PI-treated myotubes displayed decreased glucose uptake rates compared to LG and LG-I treatments. Cultures treated short- or long-term in a HG condition did not increase glucose uptake upon insulin stimulus (Figure 1C,M) but showed elevated basal rates compared to LG. We observed no significant increase in insulin-dependent vs. basal glucose uptake in all T2D-mimicking treatment groups (HG, HG-I, HG-P, HG-PI). Myotubes treated with HG-P or HG-PI showed significantly lower basal and insulin-dependent glucose uptake rates compared to HG and HG-I groups (Figure 1C,M). Myotubes treated with HM or HM-I for 24h showed a significant decrease in basal glucose uptake compared to LG or HG and no significant up-regulation of glucose uptake upon insulin stimulation. Interestingly, C2C12 myotubes treated with HM and palmitate (HM-P and HM-PI) showed a marked increase in both basal and insulin-dependent glucose uptake (Figure 1G), compared to all other treatment groups. Looking at the half-violin plots with combined data of 24h and 96h treatments, treatments including mannitol show the widest spread in values due to the stimulatory effect on glucose uptake of palmitate in combination with HM (Figure 1E), whereas in cells exposed to HG and palmitate an inhibitory effect of palmitate is apparent (Figure 1I).

H9C2 cardiac myotubes: IR occurred in all T2D-mimicking treatment groups. LG or LG-I treated control cultures showed an increase in glucose uptake upon an acute insulin stimulus (100 nM). After 24h treatment, the increase was not significant, whereas, after 96h treatment, we observed a significant rise in insulin-dependent glucose uptake compared to basal uptake (Figure 1B,L). Basal glucose uptake rates in both LG and LG-I treatment groups were similar, but insulin-dependent rates were significantly higher in LG-I compared to basal rates in LG (Figure 1B). H9C2 myotubes treated short or long-term with LG and palmitate (LG-P and LG-PI) showed significantly decreased glucose uptake rates compared to LG and LG-I. We observed similar effects on glucose uptake after short- or long-term treatments with HG-P or HG-PI (Figure 1D,N), which indicates a massive suppression of basal glucose influx and insulin insensitivity by palmitate [31]. Groups treated short- or long-term with HG or HG-I were at least partially insulin-resistant and showed a significantly higher glucose uptake compared to groups treated with high glucose and palmitate (Figure 1D,N). In contrast, osmotic control cultures treated with HM-P or HM-PI showed a remarkable increase in basal glucose

Preprints (www.preprints.org) | NOT PEER-REVIEWED | Posted: 8 November 2023 doi:10.20944/preprints202310.0319.v2

uptake compared to HM or HM-I treatment, but insulin response was suppressed (Figure 1H) even more marked than in C2C12 myotubes (Figure 1G). In summary, HM-treated groups showed markedly lower glucose uptake rates compared to LG groups (LG basal rate mean = 207.33; HM basal rate mean = 45.95). Cultures treated with HM or HM-I showed a non-significant trend towards an increase in glucose uptake upon an acute insulin stimulus (Figure 1H). Looking at the half-violin plots with combined data of 24h and 96h treatments, cells exposed to mannitol show the lowest glucose uptake rates of all treatments (Figure 1F). Overall, palmitate exerted a marked inhibitory effect on both basal and insulin-dependent glucose uptake, particularly in combination with HG treatment (Figure 1J,P).

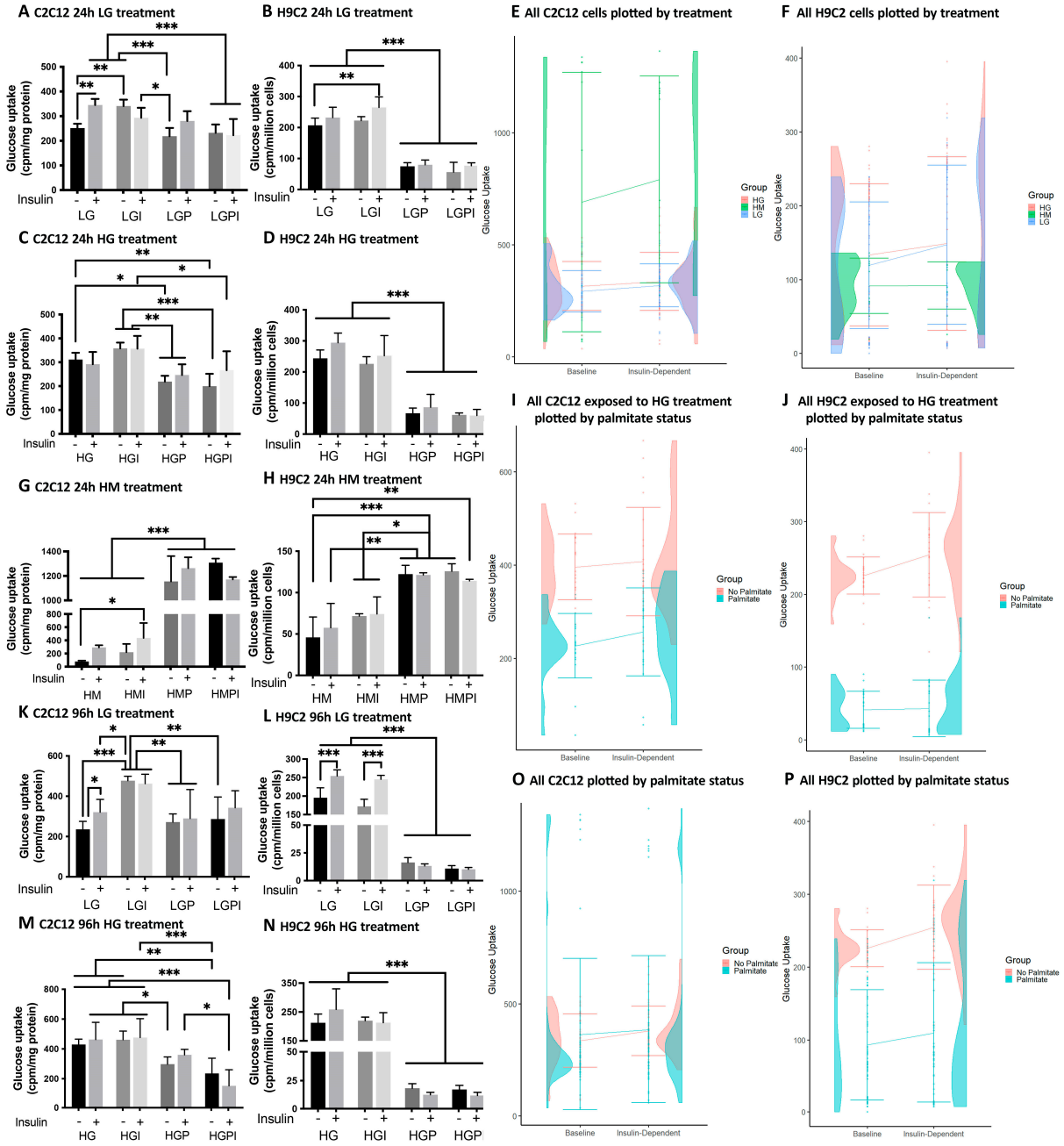

Figure 1. Basal and insulin dependent 3H-2-deoxy-glucose-uptake of C2C12 and H9C2 myotubes after 24h and 96h treatments. The effect upon an acute insulin stimulus (100 nM) was compared between different T2D-mimicking conditions and physiological (LG) and osmotic (HM) controls. IR occurred in all T2D-mimicking conditions. E, F, I, J, O, P: Half-violin plots for combined 24h and 96h baseline and insulin-dependent glucose uptake, with error bars for standard error and lines

 doi:10.20944/preprints202310.0319.v2

connecting mean glucose uptake between conditions, by group. **A:** C2C12 LG control groups after 24h treatment. **B:** H9C2 LG control groups after 24h treatment. **C:** C2C12 treated with high glucose, palmitate and insulin for 24h. **D:** H9C2 treated with HG, palmitate and insulin for 24h. **E:** All C2C12 cells plotted by treatment. **F:** All H9C2 cells by treatment. **G:** C2C12 osmotic control groups treated with HM for 24h. **H:** H9C2 osmotic control groups treated with HM for 24h. **I:** C2C12 cells receiving high glucose treatment plotted by palmitate status. **J:** H9C2 cells receiving high glucose treatment plotted by palmitate status. **K:** C2C12 96h LG treatment. **L:** H9C2 96h LG treatment. **M:** C2C12 96h HG treatments. **N:** H9C2 96h HG treatments. **O:** All C2C12 cells plotted by palmitate status. **P:** All H9C2 cells by palmitate status. Insulin (+): 100 nM acute insulin; LG: low glucose 5 mM; LGI: low glucose + 1 nM insulin; LGP: low glucose + 150 µM palmitate for C2C12 and 75 µM palmitate for H9C2; LGPI: low glucose + 150 µM palmitate for C2C12 and 75 µM palmitate for H9C2 + 1 nM insulin; HG: high glucose 25 mM; HGI: high glucose + 1 nM insulin; HGP: high glucose + 150 µM palmitate for C2C12 and 75 µM palmitate for H9C2; HGPI: high glucose + 150 µM palmitate for C2C12 and 75 µM palmitate for H9C2 + 1 nM insulin; HM: 20 mM mannitol + 5 mM glucose; HMI: 20 mM mannitol + 5 mM glucose + 1 nM insulin; HMP: 20 mM mannitol + 5 mM glucose + 150 µM palmitate for C2C12 and 75 µM palmitate for H9C2; HMPI: 20 mM mannitol + 5 mM glucose + 150 µM palmitate for C2C12 and 75 µM palmitate for H9C2 + 1 nM insulin. Basal glucose uptake and insulin dependent glucose uptake are presented as cpm per mg protein or per million cells. Values represent the means (SD); n=6 per treatment group for LG and HG treatments, n=3 per group for HM treatments. One-way ANOVA for A-D, G, H, K-N $p<0.0001$. Brackets indicate Tukey's multiple comparisons tests with *$p<0.05$, **$p<0.01$, ***$p<0.001$.

3.2. Mitochondrial Function measurements using the Agilent Seahorse XFe 96 Extracellular Flux Analyzer

In all Mito Stress Test assays with C2C12 and H9C2 myotubes, baseline relative oxygen consumption rate percentage did not differ statistically (Figure 2D,H,L,P).

3.2.1. C2C12 Myotubes

24h treatments: C2C12 myotubes treated 24h with non-physiological glucose levels (HG, HG-I, HG-P, HG-PI) showed a significant decrease in ATP-linked respiration compared to LG and LG-I controls (Figure 2A). Osmotic control cultures (HM, HM-I) showed no difference to LG control groups in maximal respiration (Figure 2B) but a significant decrease in ATP-linked respiration (Figure 2A). In all groups including insulin treatment maximal respiration rates were higher compared to treatments without insulin, but no significant changes were detectable (Figure 2B). Spare respiratory capacity rates were significantly increased in HG-I and HM-I groups compared to LG control (Figure 2C). In short-term assays with C2C12 myotubes we observed a shift towards glycolysis in all HG treated groups. HM treated groups showed a metabolic shift towards glycolysis. LG groups showed a mainly aerobic metabolism and LG-I groups were in between an aerobic and high energetic phenotype (Figure 2Q).

96h treatments: C2C12 myotubes treated 96h with high glucose (HG, HG-I) or HM-I showed a significant decrease in maximal respiration compared to LG control (Figure 2F). ATP-linked respiration of myotubes treated with HG or HM was significantly decreased (Figure 2E). Spare respiratory capacity rates were significantly decreased in HG and HG-I treated groups compared to LG. HM and HM-I treated groups displayed a lower spare respiratory capacity compared to LG-I (Figure 2G). In the XF energy map HG and HG-I treated groups showed a more glycolytic phenotype, while LG and LG-I control groups were in between an aerobic (oxidative phosphorylation) and a high energetic phenotype. HM and HM-I groups were less energetic compared to LG and less glycolytic compared to HG (Figure 2R). All respiration rates were lower after 96h treatment compared to 24h treatment, with maximal respiration rates being remarkably lower in T2D-mimicking conditions after 96h compared to 24h treatment. After 96h treatment with HG-P and HG-PI, we didn't observe significant difference to LG controls in one Mito Stress Test and therefore excluded these treatment groups in the following repetitions.

 doi:10.20944/preprints202310.0319.v2

3.2.2. H9C2 Myotubes

24h treatments: H9C2 myotubes treated 24h with high glucose in combination with insulin or palmitate (HG-I, HG-P, HG-PI) showed a significant increase in ATP-linked respiration and maximal respiration compared to LG and LG-I controls, with HG-PI groups displaying the significantly highest ATP linked respiration and respiration rates (Figure 2I,J). Spare respiratory capacity was significantly increased in treatment groups including palmitate (HG-P and HG-PI) (Figure 2K). Plotting OCR vs ECAR showed a trend towards more energetic phenotypes in T2D-mimicking conditions compared to LG controls (Figure 2S). All treatment groups utilized both glycolysis and oxidative phosphorylation to generate energy. High mannitol control cultures showed no significant differences in all respiration rates compared to LG control groups in one Mito Stress Test assay and were therefore excluded in the following assay repetitions.

96h treatments: H9C2 myotubes treated 96h with high glucose in combination with insulin or palmitate (HG-I, HG-P, HG-PI) showed a significant increase in ATP linked respiration and maximal respiration compared to LG and LGI controls (Figure 2M,N). After 96h treatment no significant changes in spare respiratory capacity was detectable (Figure 2O). Plotting OCR vs ECAR respiration rates after 96h treatment revealed LG control cultures to be more quiescent compared to 24h treatment and compared to T2D-mimicking conditions. HG, HG-I, HG-P and HG-PI treated groups showed a phenotype in between glycolysis and oxidative phosphorylation, with HG-PI being the most energetic (Figure 2T).

Preprints (www.preprints.org) | NOT PEER-REVIEWED | Posted: 8 November 2023 doi:10.20944/preprints202310.0319.v2

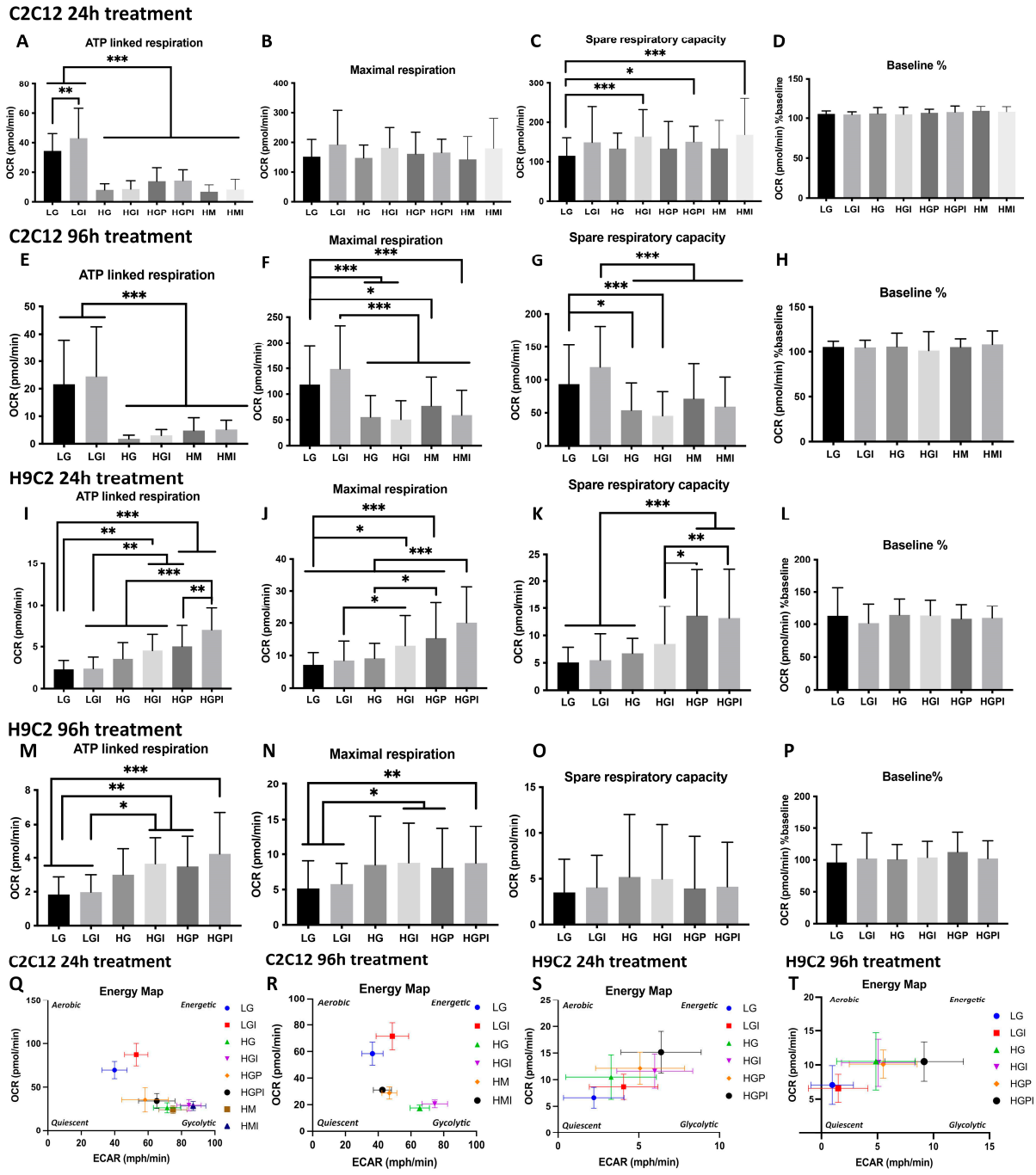

Figure 2. Plate-based oxygen consumption measurements of C2C12 (A-H, Q-R) and H9C2 (I-P, S-T) myotubes. The cells were plated at 1.2 x10^4 cells per well in XF96 microplates and differentiated for 5 days. Treatments were carried out for 24h or 96h prior to the assay. **A:** ATP-linked respiration of C2C12 myotubes after 24h treatments (row/treatment factor (Rf) F (7, 292) = 70.16, P<0.0001; column factor (Cf) F (2, 292) = 9.807, P<0.0001). **B:** Maximal respiration of C2C12 Myotubes after 24h treatments (Rf F (7, 288) = 2.206, P=0.0338; Cf F (2, 288) = 9.502, P=0.0001). **C:** Spare respiratory capacity of C2C12 Myotubes after 24h treatments (Rf F (7, 292) = 3.153, P=0.0031; Cf F (2, 292) = 15.72, P<0.0001). **D, H, L, P:** Relative oxygen consumption rate percentage (D: Rf F (7, 282) = 1.516; Cf F (2, 282) = 5.305, H: Rf F (5, 168) = 0.7035, Cf F (2, 168) = 2.439, L: Rf F (5, 146) = 0.6060, Cf F (2, 146) = 1.126, P: Rf F (5, 131) = 0.8578, Cf F (2, 131) = 0.7791). **E:** ATP-linked respiration 96h (Rf F (5, 123) = 21.21, P<0.0001; Cf F (2, 123) = 28.60, P<0.0001). **F:** Maximal respiration 96h (Rf F (5, 155) = 19.18, P<0.0001; Cf F (2, 155) = 38.29, P<0.0001). **G:** Spare respiratory capacity 96h (Rf F (5, 154) = 12.12, P<0.0001; Cf F (2, 154) = 33.39, P<0.0001). **I:** ATP-linked respiration of H9C2 myotubes after 24h treatments (Rf F (5, 139) = 23.58, P<0.0001; incubation factor F (2, 139) = 7.225, P=0.0010). **J:** Maximal respiration 24h (Rf F (5, 144) =

 doi:10.20944/preprints202310.0319.v2

20.55, P<0.0001; Cf F (2, 144) = 69.85, P<0.0001). **K:** Spare respiratory capacity 24h (Rf F (5, 135) = 15.03, P<0.0001; Cf F (2, 135) = 47.87, P<0.0001). **M:** ATP-linked respiration 96h (Rf F (5, 178) = 8.173, P<0.0001; Cf F (2, 178) = 0.2515, P=0.7779). **N:** Maximal respiration 96h (Rf F (5, 185) = 5.086, P=0.0002; Cf F (2, 185) = 47.23, P<0.0001). **O:** Spare respiratory capacity 96h (Rf F (5, 186) = 0.6408, P=0.6688; Cf F (2, 186) = 26.49, P<0.0001). **Q, R:** OCR plotted versus ECAR of C2C12 after 24h (Q) and 96h (R) treatment. **S, T:** OCR plotted versus ECAR of H9C2 after 24h (S) and 96h (T) treatment. LG: low glucose 5 mM; LGI: low glucose + 1 nM insulin; HG: high glucose 25 mM; HGI: high glucose + 1 nM insulin; HGP: high glucose + 150 μM palmitate for C2C12 and 75 μM palmitate for H9C2; HGPI: high glucose + 150 μM palmitate for C2C12 and 75 μM palmitate for H9C2 + 1 nM insulin; HM: 20 mM mannitol + 5 mM glucose; HMI: 20 mM mannitol + 5 mM glucose + 1 nM insulin. Each graph represents data of minimum three independent biological replicates and presented as means ± standard deviation, n per treatment group = 8-15 (C2C12) or 6-15 (H9C2) wells per assay. Two-way-ANOVA for row factor treatment (Rf) and column factor Seahorse assays (Cf). Significance of secondary pairwise comparisons among treatments by Tukey´s test is indicated by brackets and asterisks *: p<0.05; **: p<0.01; ***: p<0.001 in the panels.

3.3. Morphometric analyses of mitochondrial number, density, relative frequency of mitochondria with differing area and length

3.3.1. Electron Microscopy for Mitochondrial appearance.

The abnormalities caused by T2D conditions in mitochondrial function raised the question of accompanying structural abnormalities. For mitochondrial morphology analysis, the number of normal versus swollen/vacuolated mitochondria was compared after 24h treatment of C2C12 and H9C2 myotubes. Normal mitochondria were defined as indicated in Figure 3 A, swollen/vacuolated mitochondria as indicated in Figure 3B,C. HM, HG-P and HG-PI treated C2C12 myotubes showed a significantly higher fraction of swollen/vacuolated mitochondria compared to LG control (Figure 3K). The fraction of swollen/vacuolated mitochondria in HG compared to LG groups was not significantly different (Figure 3K). Compared to LG, the percentage of swollen/vacuolated mitochondria in H9C2 myotubes was higher in HM, HG and HG-PI groups (Figure 3S). Swollen mitochondria are marked as “sm” in Figure 3 in C2C12 HM, HG-P, and HG-PI treatments (Figure 3E,G,H) and H9C2 HM, HG and HG-PI treatments (Figure 3M,N,Q).

3.3.2. Mitochondrial number and density

Morphometric analyses revealed no significant changes in mitochondrial number per 10 μm2 area of cytoplasm after exposure to T2D conditions in both C2C12 (Figure 3I) and H9C2 (Figure 3O) cells.

Opposite changes in mitochondrial density between C2C12 and H9C2 cells: Morphometric analyses of mitochondrial density (area occupied by mitochondria in total area of cytoplasm) revealed a significant decrease in mitochondrial density when C2C12 cells were exposed to HG, HGP, or HGPI compared to LG (Figure 3J). In contrast, H9C2 cells showed significant increase in mitochondrial density when exposed to HGP or HGPI, compared to LG, HG (Figure 3R). These findings are consistent with the increase in ATP-linked respiration as described above.

Preprints (www.preprints.org) | NOT PEER-REVIEWED | Posted: 8 November 2023 doi:10.20944/preprints202310.0319.v2

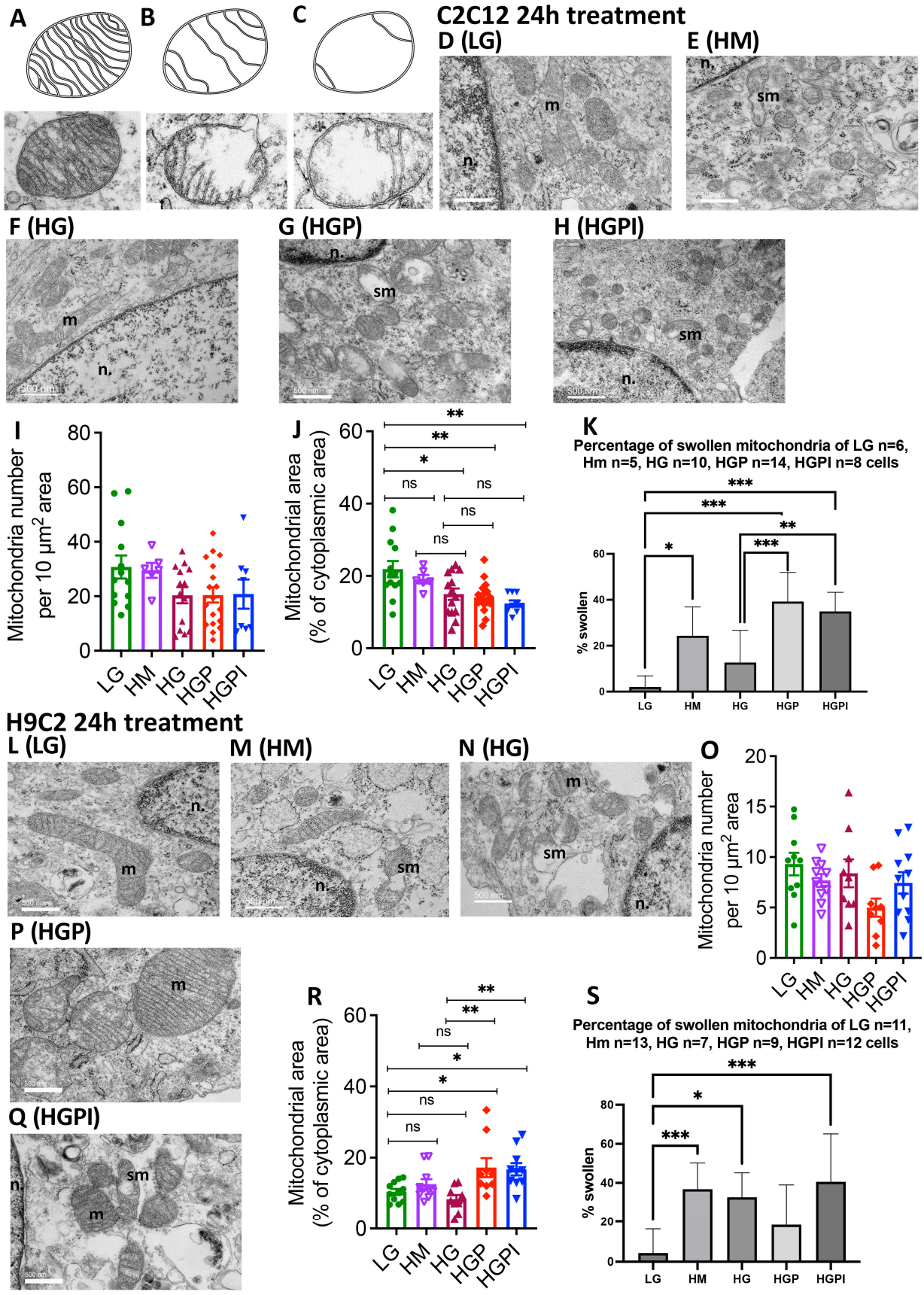

Figure 3. Mitochondrial morphology and number of C2C12 and H9C2 myotubes after 24h treatment with T2D mimicking conditions. **A:** Normal muscular mitochondria. **B-C:** Swollen mitochondria. **D-H:** Mitochondria of C2C12 myotubes after different treatments in 15kX magnification. **L-N, P, Q:** Mitochondria of H9C2 myotubes, n. = nucleus, m = normal mitochondria, sm = swollen/vacuolated

 doi:10.20944/preprints202310.0319.v2

mitochondria. **I, O:** Mitochondrial number per 10 μm2 area of cytoplasm of C2C12 (I) and H9C2 (O). **J, R:** Mitochondrial density (area occupied by mitochondria in total area of cytoplasm) in C2C12 (J) and H9C2 (R). **K, S:** Percentage of swollen mitochondria in C2C12 (K) and H9C2 (S) myotubes. LG: low glucose 5mM; HM: 20 mM mannitol + 5 mM glucose; HG: high glucose 24mM; HGP: high glucose + 150 μM palmitate for C2C12 and 75 μM palmitate for H9C2; HGPI: high glucose + 150 μM palmitate for C2C12 and 75 μM palmitate for H9C2 + 1 nM insulin. One-way ANOVA of I $p= 0.1241$; J $p=0.0007$, K + S $p<0.0001$; O $p=0.0681$; R $p=0.0009$. Tukey's tests for multiple comparisons *$p<0.05$, **$p<0.01$, ***$p<0.001$.

3.3.3. Palmitate but not HG changed relative frequency of mitochondria with respect to area and length

Morphometric analyses revealed that HG alone was not sufficient to alter the relative frequency of mitochondria with respect to area and length in both C2C12 and H9C2 cells, compared to LG (Figure 4A,J). In contrast, palmitate with high glucose caused marked changes in relative frequency of mitochondria with respect to area and length in both C2C12 and H9C2 cells compared to LG and to HM controls (Figure 4B,K,F,O), indicating that palmitate is a stronger reagent than glucose to affect mitochondrial health.

3.3.4. Insulin failed to alter palmitate-induced changes in mitochondrial health

We found no significant changes in mitochondrial area and length between HGP and HGPI groups in both C2C12 and H9C2 cells (Figure 4H,Q), indicating that palmitate in combination with HG caused profound IR in muscle cells.

Preprints (www.preprints.org) | NOT PEER-REVIEWED | Posted: 8 November 2023 doi:10.20944/preprints202310.0319.v2

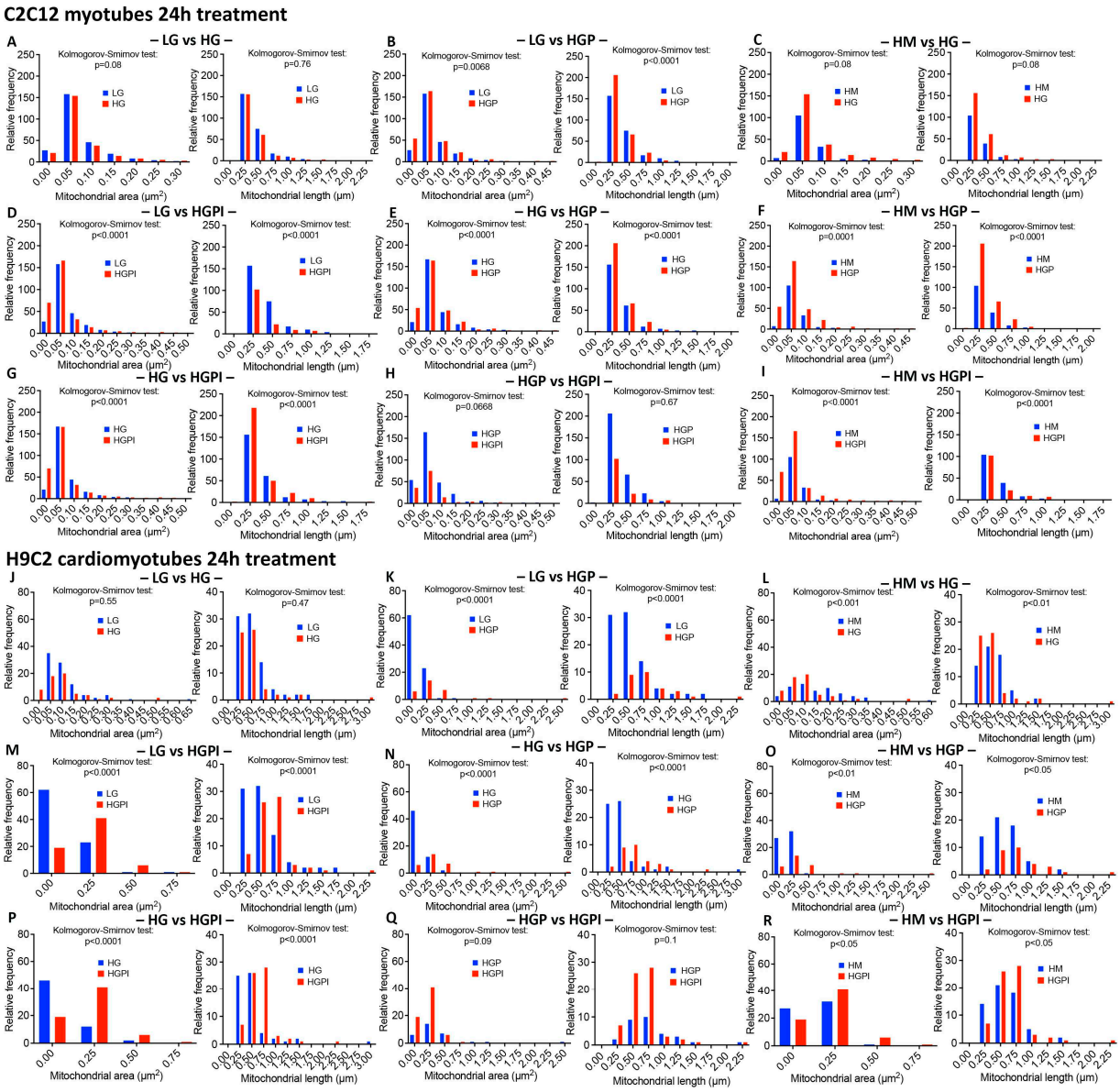

Figure 4. Relative frequency of mitochondria with respect to area and length after 24h treatment with T2D mimicking conditions. A-I C2C12 myotubes, J-R H9C2 myotubes. Kolmogorov-Smirnov-Test of mitochondrial area (µm2) and length (µm) of LG vs HG (A, J), LG vs HGP (B, K), HM vs HG (C, L); LG vs HGPI (D, M), HG vs HGP (E, N), Hm vs HGP (F, O); HG vs HGPI (G, P), HGP vs HGPI (H, Q); HM vs HGPI (I, R). LG: low glucose 5 mM; HM: 20 mM mannitol + 5 mM glucose; HG: high glucose 25 mM; HGP: high glucose + 150 µM palmitate for C2C12 and 75 µM palmitate for H9C2; HGPI: high glucose + 150 µM palmitate for C2C12 and 75 µM palmitate for H9C2 + 1 nM insulin.

4. Discussion

We observed that complex T2D in vitro modeling has significant effects on the functionality of rodent skeletal and heart muscle cells, leading to severe IR, changes in ATP-linked respiration, shifts in energetic phenotypes, and mitochondrial morphology changes, all consistent with what has been observed in the muscle of patients suffering from T2D [55]. Pre-existing in vitro models of T2D often disregard many critical and complex aspects of the disease (Table 1). The current study shows that by following some essential steps lacking in the literature, a representative in vitro model of human T2D-related changes in muscle cells can be created.

Basal glucose uptake rates were increased in both cell lines after HG treatment compared to LG, especially after long-term exposure. The gradient-driven glucose uptake might have facilitated this

 doi:10.20944/preprints202310.0319.v2

via GLUT1 instead of insulin-dependent GLUT4. McMillin et al. showed that mGLUT4 knockout mice still showed increased basal glucose uptake after chronic exposure to HG. They also found that in mouse skeletal muscle cells, GLUT1, 3, 6 or 10 almost exclusively mediate glucose uptake after chronic glucose overload [56]. Gosmanov et al. observed that, compared to 5 mM glucose exposure, HG treatment (30mM, up to 48h) of aortic endothelial cells increased GLUT1 expression and GLUT4-dependent glucose uptake, but didn't change baseline glucose uptake rates. Heilig et al. saw an 134% increase in GLUT1 mitochondrial RNA as well as a 50% increase in deoxy-glucose uptake in rat mesangial cells exposed to 20 mM glucose for 3 days, when compared to cells adapted to physiological glucose levels (8mM).

We examined mitochondrial function and metabolic phenotypes in rodent skeletal and heart muscle. Skeletal myotubes from insulin-sensitive subjects with T2D family history have decreased ATP content, consistent to previous studies showing decreased ATP and impaired mitochondrial activity in myotubes from lean offspring of T2D patients [57–59]. Mailloux et al. also observed that C2C12 myotubes exposed to 24 mM glucose for 24h showed a glycolytic phenotype and more ROS production than a low glucose control with an oxidative phenotype; however, ATP-linked respiration was not altered, indicating that those myotubes still were metabolically flexible and achieved the ATP demand via glycolysis [60]. Elkalaf et al. followed a similar approach and saw differences in maximal respiration in hyperglycemic C2C12 myotube cultures and a phenotype switch. In both studies, cells were differentiated for up to 7 days in media containing 5 mM or 25 mM glucose before any experiment [61]. Differentiating cells in high glucose might have caused an adaptation of the cells, leading to restored cellular flexibility. In the current study, cells were differentiated in low glucose levels and only exposed to high glucose for 24-96h when already differentiated, which more accurately represents the changes of T2D *in vivo*. Future experiments should include longer exposure to high glucose to investigate if, following differentiation, an adaptation to supraphysiological glucose and correspondingly non-altered ATP levels is possible.

Strongly increased respiration rates might be associated with elevated cellular stress since high glucose and palmitate levels lead to apoptosis in cardiomyocytes [62–64]. On the other hand, it can also reflect a highly energetic phenotype with increased oxidation abilities [51]. The increase in ATP-linked respiration might be associated with an increase of FA oxidation and decreased glucose utilization, which is assumed to be increased in the T2D heart in humans [65,66]. FA uptake into the heart is mainly driven by the availability in the blood stream [67]. With an oversupply in fatty acids, not only is FA oxidation increased but also detrimental lipid metabolites (i.e., ceramides) [63,68]. Reliance of the heart on FA oxidation to produce ATP might lead to oxidative stress and ischemic damage [14]. Therefore, losing the ability to switch to glycolysis combined to an increase in ROS due to the increased FA oxidation and increasing lipotoxicity contribute to both decreased ATP production and cardiac inefficiency.

In patients with T2D mitochondrial content is reduced, size and fusion are impaired, and endoplasmic reticulum stress occurs in different cell types [69]. Increased fission and impaired fusion was observed in human renal glomerular endothelial cells treated with high glucose (30 mM for 72h) [70]. A reduced number and fragmented mitochondria were found in skeletal muscle from T2D and obese subjects, as well as decreased electron transport chain activity [47]. In our study, we did observe a significant decrease in mitochondrial density in diabetic C2C12 cells, consistent with decreased ATP-linked respiration. We did not observe any significant changes in mitochondrial number per 10 μm^2 area of cytoplasm after 24h exposure to T2D mimicking conditions. Thus, it is likely that the reduction of mitochondrial number that was reported in patients suffering from T2D, is a chronic condition that will only occur in vitro after longer treatments.

H9C2 myotubes treated with T2D mimicking conditions including palmitate (HGP, HGPI) showed a significant increase in mitochondrial density compared to control, which can be a sign of increased fusion, allowing an enhanced transport of metabolites and enzymes. This observation is consistent to our Mito Stress Tests, where these cells showed increased ATP-linked respiration, confirming a better adaptability to an in vitro T2D environment of heart muscle cells.

 doi:10.20944/preprints202310.0319.v2

Both C2C12 and H9C2 myotubes treated with HM and T2D mimicking conditions showed a higher fraction of swollen/vacuolated mitochondria compared to LG controls. Mitochondrial swelling can be caused by osmotic changes in cell culture media and FA treatments but is also a known sign of apoptosis and necrosis [71]. The question remains if whether the decreased ATP-linked respiration we observed in skeletal muscle cells in the T2D environment led to imminent apoptosis and then mitochondrial swelling, or if the T2D mimicking treatments directly caused mitochondrial swelling, subsequently leading to mitochondrial dysfunction and decreased ATP turnover.

There are several limitations to consider in our studies. We chose to use the saturated FA palmitate for our investigations, as it was previously used for studies addressing IR. Even when the Western diet is dominated by saturated FAs, using only one saturated FA is not physiologically accurate since in vivo circulating FFAs are a mixture of various saturated and unsaturated FAs. For future experiments, a mixture of the most common FAs in human plasma could be used (i.e. oleic, palmitic and stearic acids) [72].

High mannitol treatments served as osmotic controls for high glucose treatments in our study, as it has been widely applied in the literature. Yet we observed some hitherto undescribed effects, especially after 96h high mannitol treatments, such as decreased ATP-linked respiration, a shift to glycolysis but decreased basal glucose uptake, and mitochondrial swelling. The mechanistic background of the effects that we observed must still be explored. Still, it can be stated that the impact of hyperosmolarity and hyperlipidemia in a hyperglycemic T2D environment appears more complex than expected.

5. Conclusions

We used two well-established skeletal and cardiac myoblast cell lines for this model and conducted differentiation with close 'normoglycemic and normoinsulinemic' conditions thus avoiding diabetogenic preconditioning before use in experiments. In the experiments, we simulated, in addition to hyperglycemia and hyperinsulinemia also, other aspects of T2D, i.e., hyperlipemia and hyperosmolarity. Despite using lower concentrations than previous studies, closer to the range seen in patients with T2D, we demonstrated a very rapid and progressive development of insulin resistance, derangements in mitochondrial metabolism and morphology with specific differences between skeletal and cardiac myotubes that parallel findings in biopsies from T2D patients. The model could potentially be extended to other tissues impacted by diabetes. Our model should therefore help to spare animal experiments and studies requiring human biopsies and has the potential for exploring pathomechanisms, defining potential new targets, and screening candidate therapeutic compounds in T2D.

Supplementary Materials: Figure S1 and Figure S2 showing light microscopy images of C2C12 and H9C2 myoblasts and -tubes in different treatment conditions to observe treatment effects.

Author Contributions: Conceptualization, E.K. and H.P.; methodology, E.K. and S.M.; validation, E.K., D.D., R.L. and S.M.; formal analysis, R.C.; investigation, E.K. and D.D., resources, H.P., D.R., S.M.; writing—original draft preparation, E. K.; writing—review and editing, E.K., H.P., R.L., D.R., D.D.; visualization, E.K.; supervision, H.P.; project administration, E. K.; funding acquisition, H.P. All authors have read and agreed to the published version of the manuscript.

Funding: This work was supported by the Department of Veterans Affairs (BX001963 to HHP) and a Research Career Scientist Award (# IK6 BX005229 to HHP).

Institutional Review Board Statement: Not applicable.

Informed Consent Statement: Not applicable.

Data Availability Statement: All data is available upon request.

Acknowledgments: We would like to thank Ying Jones from the Department of Cellular and Molecular Medicine, University of California San Diego, La Jolla, CA, USA and Ingrid Niesman from the Electron microscopy facility, SDSU, CA, USA.

Conflicts of Interest: The authors declare no conflict of interest.

References

1. Bommer C, Sagalova V, Heesemann E, et al. (2018) Global Economic Burden of Diabetes in Adults: Projections From 2015 to 2030. Diabetes care 41(5): 963-970. 10.2337/dc17-1962
2. International Diabetes Federation (2019) IDF Diabetes Atlas, 9th edn. Available at: https://www.diabetesatlas.org, Brussels, Belgium
3. Harreiter J, Roden M (2019) [Diabetes mellitus-Definition, classification, diagnosis, screening and prevention (Update 2019)]. Wiener klinische Wochenschrift 131(Suppl 1): 6-15. 10.1007/s00508-019-1450-4
4. Centers for Disease Control and Prevention (2020) National Diabetes Statistics Report, 2020. In, Atlanta, GA: , U.S. Dept of Health and Human Services
5. World Health Organization (2016) Global Report on Diabetes, Geneva, Switzerland
6. Mozaffarian D, Benjamin EJ, Go AS, et al. (2015) Heart disease and stroke statistics--2015 update: a report from the American Heart Association. Circulation 131(4): e29-322. 10.1161/cir.0000000000000152
7. Lilao-Garzón J, Valverde-Tercedor C, Muñoz-Descalzo S, Brito-Casillas Y, Wägner AM (2021) In Vivo and In Vitro Models of Diabetes: A Focus on Pregnancy. In: Islam MS (ed) Diabetes: from Research to Clinical Practice: Volume 4. Springer International Publishing, Cham, pp 553-576
8. Reed MJ, Scribner KA (1999) In-vivo and in-vitro models of type 2 diabetes in pharmaceutical drug discovery. Diabetes, Obesity and Metabolism 1(2): 75-86. https://doi.org/10.1046/j.1463-1326.1999.00014.x
9. Smith AG, Muscat GE (2005) Skeletal muscle and nuclear hormone receptors: implications for cardiovascular and metabolic disease. The international journal of biochemistry & cell biology 37(10): 2047-2063. 10.1016/j.biocel.2005.03.002
10. Tumova J, Andel M, Trnka J (2016) Excess of free fatty acids as a cause of metabolic dysfunction in skeletal muscle. Physiological research 65(2): 193-207. 10.33549/physiolres.932993
11. Wong CY, Al-Salami H, Dass CR (2020) C2C12 cell model: its role in understanding of insulin resistance at the molecular level and pharmaceutical development at the preclinical stage. Journal of Pharmacy and Pharmacology 72(12): 1667-1693. https://doi.org/10.1111/jphp.13359
12. Ashrafian H, Frenneaux MP, Opie LH (2007) Metabolic Mechanisms in Heart Failure. Circulation 116(4): 434-448. doi:10.1161/CIRCULATIONAHA.107.702795
13. Stanley WC, Recchia FA, Lopaschuk GD (2005) Myocardial Substrate Metabolism in the Normal and Failing Heart. Physiological Reviews 85(3): 1093-1129. 10.1152/physrev.00006.2004
14. Carpentier AC (2018) Abnormal Myocardial Dietary Fatty Acid Metabolism and Diabetic Cardiomyopathy. The Canadian journal of cardiology 34(5): 605-614. 10.1016/j.cjca.2017.12.029
15. Westermeier F, Navarro-Marquez M, Lopez-Crisosto C, et al. (2015) Defective insulin signaling and mitochondrial dynamics in diabetic cardiomyopathy. Biochimica et biophysica acta 1853(5): 1113-1118. 10.1016/j.bbamcr.2015.02.005
16. Amaral N, Okonko DO (2015) Metabolic abnormalities of the heart in type II diabetes. Diabetes & vascular disease research 12(4): 239-248. 10.1177/1479164115580936
17. Kimes BW, Brandt BL (1976) Properties of a clonal muscle cell line from rat heart. Experimental cell research 98(2): 367-381. 10.1016/0014-4827(76)90447-x
18. Watkins SJ, Borthwick GM, Arthur HM (2011) The H9C2 cell line and primary neonatal cardiomyocyte cells show similar hypertrophic responses in vitro. In Vitro Cell Dev Biol Anim 47(2): 125-131. 10.1007/s11626-010-9368-1
19. Zordoky BN, El-Kadi AO (2007) H9c2 cell line is a valuable in vitro model to study the drug metabolizing enzymes in the heart. Journal of pharmacological and toxicological methods 56(3): 317-322. 10.1016/j.vascn.2007.06.001
20. Chavez JA, Summers SA (2003) Characterizing the effects of saturated fatty acids on insulin signaling and ceramide and diacylglycerol accumulation in 3T3-L1 adipocytes and C2C12 myotubes. Archives of Biochemistry and Biophysics 419(2): 101-109. https://doi.org/10.1016/j.abb.2003.08.020
21. Krako Jakovljevic N, Pavlovic K, Zujovic T, et al. (2021) In vitro models of insulin resistance: Mitochondrial coupling is differently affected in liver and muscle cells. Mitochondrion 61: 165-173. https://doi.org/10.1016/j.mito.2021.10.001
22. Regazzetti C, Peraldi P, Grémeaux T, et al. (2009) Hypoxia Decreases Insulin Signaling Pathways in Adipocytes. Diabetes 58(1): 95-103. 10.2337/db08-0457

23. Sakoda H, Ogihara T, Anai M, et al. (2000) Dexamethasone-induced insulin resistance in 3T3-L1 adipocytes is due to inhibition of glucose transport rather than insulin signal transduction. Diabetes 49(10): 1700-1708. 10.2337/diabetes.49.10.1700
24. Nelson BA, Robinson KA, Buse MG (2000) High glucose and glucosamine induce insulin resistance via different mechanisms in 3T3-L1 adipocytes. Diabetes 49(6): 981-991
25. Dohl J, Foldi J, Heller J, Gasier HG, Deuster PA, Yu T (2018) Acclimation of C2C12 myoblasts to physiological glucose concentrations for in vitro diabetes research. Life Sciences 211: 238-244. https://doi.org/10.1016/j.lfs.2018.09.041
26. Yang M, Wei D, Mo C, et al. (2013) Saturated fatty acid palmitate-induced insulin resistance is accompanied with myotube loss and the impaired expression of health benefit myokine genes in C2C12 myotubes. Lipids in health and disease 12: 104. 10.1186/1476-511x-12-104
27. Chanon S, Durand C, Vieille-Marchiset A, et al. (2017) Glucose Uptake Measurement and Response to Insulin Stimulation in In Vitro Cultured Human Primary Myotubes. J Vis Exp(124): 55743. 10.3791/55743
28. Feng CC, Pandey S, Lin CY, et al. (2018) Cardiac apoptosis induced under high glucose condition involves activation of IGF2R signaling in H9c2 cardiomyoblasts and streptozotocin-induced diabetic rat hearts. Biomedicine & pharmacotherapy = Biomedecine & pharmacotherapie 97: 880-885. 10.1016/j.biopha.2017.11.020
29. Ding W, Chang WG, Guo XC, et al. (2019) Exenatide Protects Against Cardiac Dysfunction by Attenuating Oxidative Stress in the Diabetic Mouse Heart. Frontiers in endocrinology 10: 202. 10.3389/fendo.2019.00202
30. Ha H, Pak Y (2005) Modulation of the caveolin-3 and Akt status in caveolae by insulin resistance in H9c2 cardiomyoblasts. Experimental & molecular medicine 37(3): 169-178. 10.1038/emm.2005.23
31. Chang W, Chen L, Hatch GM (2016) Berberine treatment attenuates the palmitate-mediated inhibition of glucose uptake and consumption through increased 1,2,3-triacyl-sn-glycerol synthesis and accumulation in H9c2 cardiomyocytes. Biochimica et Biophysica Acta (BBA)—Molecular and Cell Biology of Lipids 1861(4): 352-362. https://doi.org/10.1016/j.bbalip.2015.12.017
32. Eckel RH, Grundy SM, Zimmet PZ (2005) The metabolic syndrome. Lancet (London, England) 365(9468): 1415-1428. 10.1016/s0140-6736(05)66378-7
33. Delarue J, Magnan C (2007) Free fatty acids and insulin resistance. Current opinion in clinical nutrition and metabolic care 10(2): 142-148. 10.1097/MCO.0b013e328042ba90
34. Katsarou A, Gudbjörnsdottir S, Rawshani A, et al. (2017) Type 1 diabetes mellitus. Nature Reviews Disease Primers 3(1): 17016. 10.1038/nrdp.2017.16
35. American Diabetes Association (2010) Diagnosis and classification of diabetes mellitus. Diabetes care 33 Suppl 1(Suppl 1): S62-S69. 10.2337/dc10-S062
36. World Health Organization Mean fasting blood glucose. Available from https://www.who.int/data/gho/indicator-metadata-registry/imr-details/2380. Accessed 16.02. 2021
37. Zhou B, Lu Y, Hajifathalian K, et al. (2016) Worldwide trends in diabetes since 1980: a pooled analysis of 751 population-based studies with 4·4 million participants. The Lancet 387(10027): 1513-1530. 10.1016/S0140-6736(16)00618-8
38. Hsu HC, Chen CY, Lee BC, Chen MF (2016) High-fat diet induces cardiomyocyte apoptosis via the inhibition of autophagy. European journal of nutrition 55(7): 2245-2254. 10.1007/s00394-015-1034-7
39. Zou L, Li X, Wu N, Jia P, Liu C, Jia D (2017) Palmitate induces myocardial lipotoxic injury via the endoplasmic reticulum stress-mediated apoptosis pathway. Molecular medicine reports 16(5): 6934-6939. 10.3892/mmr.2017.7404
40. Abdelmagid SA, Clarke SE, Nielsen DE, et al. (2015) Comprehensive profiling of plasma fatty acid concentrations in young healthy Canadian adults. PLoS One 10(2): e0116195. 10.1371/journal.pone.0116195
41. Nawrocki A, Górski J (2004) Effect of plasma free fatty acid concentration on the content and composition of the free fatty acid fraction in rat skeletal muscles. Hormone and metabolic research = Hormon- und Stoffwechselforschung = Hormones et metabolisme 36(9): 601-606. 10.1055/s-2004-825922
42. Mangnall D, Bruce C, Fraser RB (1993) Insulin-stimulated glucose uptake in C2C12 myoblasts. Biochemical Society transactions 21(4): 438s. 10.1042/bst021438s
43. Conejo R, Lorenzo M (2001) Insulin signaling leading to proliferation, survival, and membrane ruffling in C2C12 myoblasts. Journal of Cellular Physiology 187(1): 96-108. https://doi.org/10.1002/1097-4652(2001)9999:9999<::AID-JCP1058>3.0.CO;2-V

44. Patten V, Chabaesele I, Sishi B, Vuuren D (2017) Cardiomyocyte differentiation: Experience and observations from 2 laboratories. Journal of the South African Heart Association (SA Heart) 14: 96-107. 10.24170/14-2-2498
45. Lopaschuk GD, Jaswal JS (2010) Energy metabolic phenotype of the cardiomyocyte during development, differentiation, and postnatal maturation. Journal of cardiovascular pharmacology 56(2): 130-140. 10.1097/FJC.0b013e3181e74a14
46. Nobuhara M, Saotome M, Watanabe T, et al. (2013) Mitochondrial dysfunction caused by saturated fatty acid loading induces myocardial insulin-resistance in differentiated H9c2 myocytes: a novel ex vivo myocardial insulin-resistance model. Experimental cell research 319(7): 955-966. 10.1016/j.yexcr.2013.02.004
47. Kelley DE, He J, Menshikova EV, Ritov VB (2002) Dysfunction of mitochondria in human skeletal muscle in type 2 diabetes. Diabetes 51(10): 2944-2950
48. Kim JY, Hickner RC, Cortright RL, Dohm GL, Houmard JA (2000) Lipid oxidation is reduced in obese human skeletal muscle. American journal of physiology Endocrinology and metabolism 279(5): E1039-1044. 10.1152/ajpendo.2000.279.5.E1039
49. Li P, Oh DY, Bandyopadhyay G, et al. (2015) LTB4 promotes insulin resistance in obese mice by acting on macrophages, hepatocytes and myocytes. Nat Med 21(3): 239-247. 10.1038/nm.3800
50. Serrage HJ, Joanisse S, Cooper PR, et al. (2019) Differential responses of myoblasts and myotubes to photobiomodulation are associated with mitochondrial number. J Biophotonics 12(6): e201800411. 10.1002/jbio.201800411
51. Divakaruni AS, Paradyse A, Ferrick DA, Murphy AN, Jastroch M (2014) Chapter Sixteen—Analysis and Interpretation of Microplate-Based Oxygen Consumption and pH Data. In: Murphy AN, Chan DC (eds) Methods in Enzymology. Vol 547. Academic Press, pp 309-354
52. Patel HH, Zhang S, Murray F, et al. (2007) Increased smooth muscle cell expression of caveolin-1 and caveolae contribute to the pathophysiology of idiopathic pulmonary arterial hypertension. FASEB J 21(11): 2970-2979. 10.1096/fj.07-8424com
53. Pasqua T, Mahata S, Bandyopadhyay GK, et al. (2016) Impact of Chromogranin A deficiency on catecholamine storage, catecholamine granule morphology and chromaffin cell energy metabolism in vivo. Cell and Tissue Research 363(3): 693-712. 10.1007/s00441-015-2316-3
54. Zhang Q, Kong X, Yuan H, Guan H, Li Y, Niu Y (2019) Mangiferin Improved Palmitate-Induced-Insulin Resistance by Promoting Free Fatty Acid Metabolism in HepG2 and C2C12 Cells via PPARα: Mangiferin Improved Insulin Resistance. J Diabetes Res 2019: 2052675. 10.1155/2019/2052675
55. Fealy CE, Mulya A, Axelrod CL, Kirwan JP (2018) Mitochondrial dynamics in skeletal muscle insulin resistance and type 2 diabetes. Transl Res 202: 69-82. 10.1016/j.trsl.2018.07.011
56. McMillin SL, Schmidt DL, Kahn BB, Witczak CA (2017) GLUT4 Is Not Necessary for Overload-Induced Glucose Uptake or Hypertrophic Growth in Mouse Skeletal Muscle. Diabetes 66(6): 1491-1500. 10.2337/db16-1075
57. Petersen KF, Dufour S, Befroy D, Garcia R, Shulman GI (2004) Impaired mitochondrial activity in the insulin-resistant offspring of patients with type 2 diabetes. The New England journal of medicine 350(7): 664-671. 10.1056/NEJMoa031314
58. Morino K, Petersen KF, Dufour S, et al. (2005) Reduced mitochondrial density and increased IRS-1 serine phosphorylation in muscle of insulin-resistant offspring of type 2 diabetic parents. J Clin Invest 115(12): 3587-3593. 10.1172/JCI25151
59. Befroy DE, Petersen KF, Dufour S, et al. (2007) Impaired Mitochondrial Substrate Oxidation in Muscle of Insulin-Resistant Offspring of Type 2 Diabetic Patients. Diabetes 56(5): 1376-1381. 10.2337/db06-0783
60. Mailloux RJ, Harper M-E (2010) Glucose regulates enzymatic sources of mitochondrial NADPH in skeletal muscle cells; a novel role for glucose-6-phosphate dehydrogenase. The FASEB Journal 24(7): 2495-2506. https://doi.org/10.1096/fj.09-151803
61. Elkalaf M, Anděl M, Trnka J (2013) Low glucose but not galactose enhances oxidative mitochondrial metabolism in C2C12 myoblasts and myotubes. PLoS One 8(8): e70772-e70772. 10.1371/journal.pone.0070772
62. Wang X, McLennan SV, Allen TJ, Tsoutsman T, Semsarian C, Twigg SM (2009) Adverse effects of high glucose and free fatty acid on cardiomyocytes are mediated by connective tissue growth factor. American Journal of Physiology-Cell Physiology 297(6): C1490-C1500. 10.1152/ajpcell.00049.2009

63. Hickson-Bick DL, Buja LM, McMillin JB (2000) Palmitate-mediated alterations in the fatty acid metabolism of rat neonatal cardiac myocytes. J Mol Cell Cardiol 32(3): 511-519. 10.1006/jmcc.1999.1098
64. Nishi H, Higashihara T, Inagi R (2019) Lipotoxicity in Kidney, Heart, and Skeletal Muscle Dysfunction. Nutrients 11(7). 10.3390/nu11071664
65. Lisa CH, Kieran C (2011) Metabolism, hypoxia and the diabetic heart. Journal of Molecular and Cellular Cardiology 50(4): 598-605. https://doi.org/10.1016/j.yjmcc.2011.01.007
66. Barsotti A, Giannoni A, Di Napoli P, Emdin M (2009) Energy metabolism in the normal and in the diabetic heart. Current pharmaceutical design 15(8): 836-840. 10.2174/138161209787582066
67. An D, Rodrigues B (2006) Role of changes in cardiac metabolism in development of diabetic cardiomyopathy. American Journal of Physiology-Heart and Circulatory Physiology 291(4): H1489-H1506. 10.1152/ajpheart.00278.2006
68. Sharma S, Adrogue JV, Golfman L, et al. (2004) Intramyocardial lipid accumulation in the failing human heart resembles the lipotoxic rat heart. The FASEB Journal 18(14): 1692-1700. https://doi.org/10.1096/fj.04-2263com
69. Zorzano A, Liesa M, Palacín M (2009) Role of mitochondrial dynamics proteins in the pathophysiology of obesity and type 2 diabetes. The international journal of biochemistry & cell biology 41(10): 1846-1854. 10.1016/j.biocel.2009.02.004
70. Chen W, Xiang H, Chen R, et al. (2019) S1PR2 antagonist ameliorate high glucose-induced fission and dysfunction of mitochondria in HRGECs via regulating ROCK1. BMC Nephrology 20(1): 135. 10.1186/s12882-019-1323-0
71. Davis MA, Jeffery EH (2002) 4—Organelle Biochemistry and Regulation of Cell Death. In: Haschek WM, Rousseaux CG, Wallig MA (eds) Handbook of Toxicologic Pathology (Second Edition). Academic Press, San Diego, pp 67-81
72. Quehenberger O, Armando AM, Brown AH, et al. (2010) Lipidomics reveals a remarkable diversity of lipids in human plasma1[S]. Journal of Lipid Research 51(11): 3299-3305. https://doi.org/10.1194/jlr.M009449